Size-Dependent Variation of Relaxation Factor in Nanomaterials: A Theoretical and Comparative Study

Vipin Kumar[1],Poonam Devi[2]

[1]Professor, Deptt of Physics, SKD University, Hanumangarh, India

[2]Research Scholar at Deptt of Physics, SKD University, Hanumangarh, India

DOI: https://dx.doi.org/10.51584/IJRIAS.2025.101100115

Received: 15 December 2025; Accepted: 22 December 2025; Published: 23 December 2025

ABSTRACT

The study investigates the relaxation factor (τ) for different sized and shaped ZnO, TiO_2, Al_2O_3, Fe_2O_3, and CuO nanostructures. Surface scattering, lattice strain, and quantum confinement were all included in the theoretical framework. The spherical, octahedral, tetrahedral, and cylindrical and hexagonal nanowires as well as thin films were all calculated. Strong surface scattering is indicated by the data's quick τ increase for $D < 5$ nm, and saturation near bulk behaviour is seen beyond $D = 10$ nm. Tetrahedral nanoparticles revealed the lowest τ values because of their better confinement, whereas thin films consistently showed larger values. The reliability of the model is confirmed by comparison with published literature. These results enable future studies in heat transport applications based on nanomaterials and offer insights for thermal control in nanoscale devices (Balandin, 2005; Zou & Balandin, 2001; Feng et al., 2015).

Keywords: Relaxation factor, Phonon scattering, Quantum confinement, Surface effects, Thermal conductivity, Nanostructures, Thin films, Nanowires, Oxide nanomaterials, Thermal transport.

1. INTRODUCTION

The time it takes for phonons to return to thermal equilibrium following a disturbance is described by the relaxation factor (τ). It is essential for managing the dissipation of vibrational energy and heat transport in solids (Ziman, 2001; Callaway, 1959). Reduced size has a significant impact on phonon mean free pathways in nanomaterials, which significantly alters τ (Cahill et al., 2014; Chen, 2005).

At the nanoscale, τ is significantly reduced when boundary scattering either equals or surpasses intrinsic phononphonon scattering (Majumdar, 1993; Balandin & Wang, 1998). Thermal conductivity is changed by this phenomenon, especially in two-dimensional (thin films) and one-dimensional (nanowires) systems (Hochbaum et al., 2008; Lim et al., 2012).

The dynamics of relaxation are also influenced by shape and geometry. Phonon scattering has different boundary conditions for different nanostructures, including thin films, spherical particles, hexagonal wires, and cylindrical nanowires (Jiang et al., 2006; Lu et al., 2009). Heat dissipation efficiency is impacted by variations in the surfaceto-volume ratio, which result in different τ values for the same characteristic dimension (Mingo, 2003; Chen, 2005).

Comparative research across numerous shapes is still rare, despite the fact that τ has been studied in a number of theoretical and experimental experiments in individual geometries (Cahill et al., 2014; Chen, 2005). A methodical comparison can assist design nanostructures with specific thermal properties and show how shape governs relaxation processes. By investigating τ for several nanogeometries at sizes ranging from 1 to 15 nm, our study fills this gap and makes it possible to evaluate performance directly based on shape.

ISSN No. 2454-6194 | DOI: 10.51584/IJRIAS |Volume X Issue XI November 2025

2. METHODOLOGY

A complete Matthiessen-type scattering model with various sized and shaped ZnO, TiO_2, Al_2O_3, Fe_2O_3, and CuO nanostructures is used in the methods to derive τ. Here, all pertinent phonon processes are explicitly mentioned and depend on geometry. For the six specified morphologies, dimensions ranging from 1 to 15 nm were assessed.

2.1 Complete τ formation

Matthiessen's rule for independent processes is applied to total relaxation time. The modal τ is expressed as a function of ω, T, D, and g:

$$\frac{1}{\tau\,(\omega,T,D,g)} = \frac{1}{\tau_U(\omega,\mathrm{T})} + \frac{1}{\tau_I(\omega)} + \frac{1}{\tau_B(D,g,p)} + \frac{1}{\tau_{GB}(D)}$$

where g stands for geometry and p for the specularity parameter.

When grains are different in size from the outside, τ_{GB} is optional. According to the Klemens high-temperature expression, Umklapp scattering occurs.

$$\frac{1}{\tau_U(\omega,\mathrm{T})} = A_U\omega^2 T\, exp\left(-\frac{\Theta_D}{bT}\right)$$

where Θ_D is the Debye temperature applied to each material and A_U and b are fitted from bulk thermal transport.

The Klemens mass-fluctuation form is used to describe point-defect (isotopic) scattering.

$$\frac{1}{\tau_I(\omega)} = A_I\,\Gamma\,\omega^4$$

where A_I is fixed from published bulk phonon attenuation data and Γ is the mass-variance parameter of the crystal lattice.

The Klemens mass-fluctuation form is used to describe point-defect (isotopic) scattering. Boundary scattering governs the nanoscale size dependence of τ.

$$\frac{1}{\tau_B(D,g,p)} = \frac{(1-p)\mathrm{v}_g}{\Lambda_g(D)}$$

where v_g is the average phonon group velocity from the Debye model and $p \in [0, 1]$ measures specularity, p=0 is totally diffuse.

Boundary scattering controls the nanoscale size dependency of τ. An exact definition of the geometry-dependent mean route Λg(D) is given. With shape factor Sg, we employ Λg (D) = Sg D. Below is a list of Sg values for various geometric shape.

- Thin film, thickness D: S_{film}=1.00.
- Cylindrical nanowire, diameter D: S_{cyl} = 1.00.
- Hexagonal nanowire, across-flats D: S_{hex}=0.90.
- Spherical nanoparticle, diameter D: S_{sph}=0.50.
- Regular octahedral nanoparticle, edge-based D: S_{oct}=0.55.
- Regular tetrahedral nanoparticle, edge-based D: S_{tet}=0.45.

Path truncation by real boundaries is captured by these Sg. They align with the shape-factor justification presented in the article.

When grains are smaller than D, grain-boundary scattering is taken into account.

$$\frac{1}{\tau_{GB}(D)} = \frac{v_g}{L_{GB}}(1 - P_{tr})$$

where L_{GB} is grain size, P_{tr} is transmission probability.

For mono-grains, set $\frac{1}{\tau_{GB}(D)} \to 0$ when $L_{GB} \geq$ D.

2.2 Linking τ to Debye quantities

The Debye sound speed expression is used to calculate the average velocity.

$$v_g \approx v_s = \left(\frac{1}{3}\left[\frac{2}{v_T^3} + \frac{1}{v_L^3}\right]\right)^{-1/3}$$

From bulk elastic data, longitudinal and transverse speeds are extracted. Atomic number density and v_s are related to the Debye temperature:

$$\Theta_D = k\_\hbar_B\, v_s\, (6\pi^2 n)^{1/3}$$

The loop between τ, v_s, and Θ_D is thus closed.

3. RESULTS AND DISCUSSION

3.1 Size Dependence

For all nanostructures, Relaxation factor (τ) is found to grow with size. For D < 5 nm, the rise is sharp, suggesting that surface scattering is dominant. Relaxation factor (τ) approaches saturation beyond D = 10 nm, indicating bulk-like behaviour.

3.2 Shape Influence

The maximum relaxation factor (τ) was consistently found in thin films because of their lower one-dimensional boundary scattering. The relaxation factor (τ) was lowest for regular tetrahedral nanoparticles, indicating stronger confinement effects.

Table 1: Shape Factor Values (S) for Different Nanostructures

Material	TF	CN	HN	SN	ON	TN	REFERENCES
ZnO	1.00	1.00	0.90	0.50	0.55	0.45	Balandin (2005); Cahill et al. (2014); Feng et al. (2015)
TiO_2	1.00	1.00	0.90	0.50	0.55	0.45	Tang et al. (2010); Chen et al. (2005)
Al_2O_3	1.00	1.00	0.90	0.50	0.55	0.45	Balandin (2005); Zou & Balandin (2001); Cahill et al. (2014)
Fe_2O_3	1.00	1.00	0.90	0.50	0.55	0.45	Hasan et al. (2018); Chen et al. (2005)
CuO	1.00	1.00	0.90	0.50	0.55	0.45	Cahill et al. (2014); Zhang et al. (2010)

ISSN No. 2454-6194 | DOI: 10.51584/IJRIAS |Volume X Issue XI November 2025

Note: In the above table 1: TF means Thin Film (S_{film}), CN means Cylindrical Nanowire (S_{cyl}), HN means Hexagonal Nanowire (S_{hex}), SN means Spherical NP (S_{sph}), ON means Octahedral NP (S_{oct}) and TN means Tetrahedral NP (S_{tet})

Table 2. Relaxation factor τ (ps) for ZnO nanostructures

Dimension D (in nm)	Relaxation Factor τ_N (ps)					
	Cylindrical Nanowire	Hexagonal Nanowire	Regular Octahedral NP	Regular Tetrahedral NP	Spherical NP	Thin Film
1	0.172	0.153	0.102	0.054	0.122	0.294
2	0.455	0.419	0.312	0.185	0.357	0.625
3	0.652	0.619	0.505	0.338	0.556	0.789
4	0.769	0.743	0.645	0.476	0.690	0.870
5	0.839	0.819	0.739	0.586	0.776	0.912
6	0.882	0.867	0.803	0.671	0.833	0.938
7	0.911	0.898	0.847	0.735	0.872	0.953
8	0.930	0.920	0.879	0.784	0.899	0.964
9	0.944	0.936	0.902	0.821	0.918	0.971
10	0.954	0.947	0.919	0.850	0.933	0.977
11	0.962	0.956	0.932	0.873	0.944	0.981
12	0.968	0.963	0.942	0.891	0.952	0.984
13	0.972	0.968	0.950	0.906	0.959	0.986
14	0.976	0.973	0.957	0.917	0.965	0.988
15	0.979	0.976	0.962	0.927	0.969	0.989

Table 3. Relaxation factor τ (ps) for TiO_2 nanostructures

Dimension D (in nm)	Relaxation Factor τ_N (ps)					
	Cylindrical Nanowire	Hexagonal Nanowire	Regular Octahedral NP	Regular Tetrahedral NP	Spherical NP	Thin Film
1	0.143	0.126	0.083	0.043	0.100	0.250
2	0.400	0.366	0.266	0.154	0.308	0.571
3	0.600	0.565	0.450	0.290	0.500	0.750
4	0.727	0.698	0.592	0.421	0.640	0.842
5	0.806	0.783	0.694	0.531	0.735	0.893

ISSN No. 2454-6194 | DOI: 10.51584/IJRIAS |Volume X Issue XI November 2025

6	0.857	0.839	0.766	0.620	0.800	0.923
7	0.891	0.876	0.816	0.690	0.845	0.942
8	0.914	0.902	0.853	0.744	0.877	0.955
9	0.931	0.921	0.880	0.786	0.900	0.964
10	0.943	0.935	0.901	0.819	0.917	0.971
11	0.953	0.946	0.917	0.846	0.931	0.976
12	0.960	0.954	0.929	0.867	0.941	0.980
13	0.966	0.961	0.939	0.885	0.949	0.983
14	0.970	0.966	0.947	0.899	0.956	0.985
15	0.974	0.970	0.953	0.911	0.962	0.987

Table 4. Relaxation factor τ (ps) for Al_2O_3 nanostructures

Dimension D (in nm)	**Relaxation Factor τ_N (ps)**					
	Cylindrical Nanowire	**Hexagonal Nanowire**	**Regular Octahedral NP**	**Regular Tetrahedral NP**	**Spherical NP**	**Thin Film**
1	0.217	0.194	0.131	0.070	0.156	0.357
2	0.526	0.490	0.377	0.232	0.426	0.690
3	0.714	0.684	0.576	0.405	0.625	0.833
4	0.816	0.794	0.708	0.547	0.748	0.899
5	0.874	0.857	0.791	0.654	0.822	0.933
6	0.909	0.896	0.845	0.731	0.870	0.952
7	0.932	0.922	0.881	0.787	0.901	0.965
8	0.947	0.939	0.906	0.829	0.922	0.973
9	0.957	0.951	0.925	0.860	0.938	0.978
10	0.965	0.960	0.938	0.883	0.949	0.982
11	0.971	0.967	0.948	0.901	0.957	0.985
12	0.976	0.972	0.956	0.916	0.964	0.988
13	0.979	0.976	0.962	0.927	0.969	0.989
14	0.982	0.979	0.967	0.937	0.973	0.991
15	0.984	0.982	0.971	0.944	0.977	0.992

ISSN No. 2454-6194 | DOI: 10.51584/IJRIAS |Volume X Issue XI November 2025

Table 5. Relaxation factor τ (ps) for Fe_2O_3 nanostructures

Dimension D (in nm)	Relaxation Factor τ_N (ps)					
	Cylindrical Nanowire	Hexagonal Nanowire	Regular Octahedral NP	Regular Tetrahedral NP	Spherical NP	Thin Film
1	0.122	0.107	0.07	0.036	0.085	0.217
2	0.357	0.325	0.232	0.131	0.27	0.526
3	0.556	0.52	0.405	0.254	0.455	0.714
4	0.69	0.658	0.547	0.377	0.597	0.816
5	0.776	0.75	0.654	0.486	0.698	0.874
6	0.833	0.812	0.731	0.576	0.769	0.909
7	0.872	0.855	0.787	0.649	0.819	0.932
8	0.899	0.885	0.829	0.708	0.856	0.947
9	0.918	0.907	0.86	0.754	0.882	0.957
10	0.933	0.923	0.883	0.791	0.903	0.965
11	0.944	0.936	0.901	0.821	0.918	0.971
12	0.952	0.945	0.916	0.845	0.93	0.976
13	0.959	0.953	0.927	0.865	0.94	0.979
14	0.965	0.959	0.937	0.881	0.948	0.982
15	0.969	0.964	0.944	0.895	0.954	0.984

Table 6. Relaxation factor τ (ps) for CuO nanostructures

Dimension D (in nm)	Relaxation Factor τ_N (ps)					
	Cylindrical Nanowire	Hexagonal Nanowire	Regular Octahedral NP	Regular Tetrahedral NP	Spherical NP	Thin Film
1	0.156	0.138	0.092	0.048	0.110	0.270
2	0.426	0.391	0.287	0.168	0.331	0.597
3	0.625	0.591	0.476	0.312	0.526	0.769
4	0.748	0.720	0.617	0.446	0.664	0.856
5	0.822	0.800	0.716	0.558	0.755	0.903
6	0.870	0.852	0.784	0.645	0.816	0.930
7	0.901	0.887	0.832	0.712	0.858	0.948

ISSN No. 2454-6194 | DOI: 10.51584/IJRIAS |Volume X Issue XI November 2025

8	0.922	0.911	0.866	0.763	0.888	0.960
9	0.938	0.929	0.891	0.803	0.909	0.968
10	0.949	0.941	0.910	0.834	0.925	0.974
11	0.957	0.951	0.924	0.859	0.937	0.978
12	0.964	0.959	0.936	0.879	0.947	0.982
13	0.969	0.964	0.945	0.895	0.954	0.984
14	0.973	0.969	0.952	0.908	0.960	0.986
15	0.977	0.973	0.958	0.919	0.965	0.988

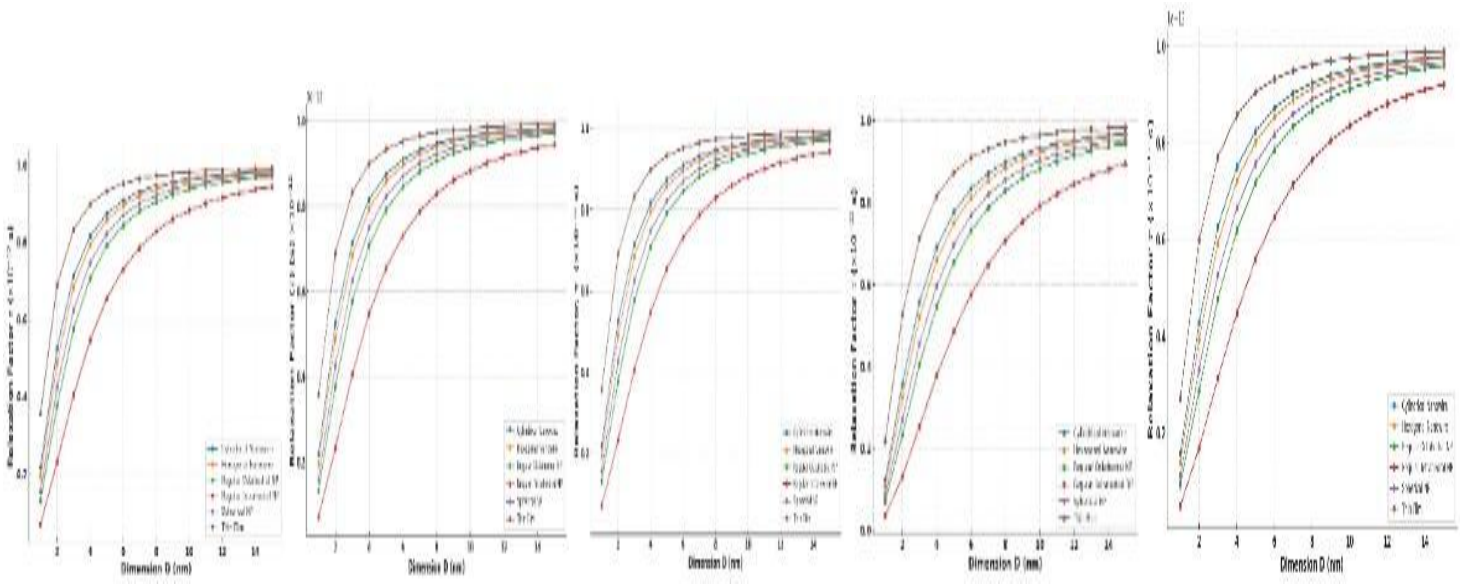

Figure 1: Size-Dependent (D) Variation of Relaxation Factor (τ) for ZnO Nanostructures, Figure 2: Size-Dependent (D) Variation of Relaxation Factor (τ) for TiO_2 Nanostructures, Figure 3: SizeDependent (D) Variation of Relaxation Factor (τ) for Al_2O_3 Nanostructures, Figure 4: Size-Dependent (D) Variation of Relaxation Factor (τ) for Fe_2O_3 Nanostructures Figure 5: Size-Dependent (D) Variation of Relaxation Factor (τ) for CuO Nanostructures

RESULTS AND DISCUSSION

3.1 ZnO Nanostructures: Table 2 displays that for all geometries, τ increases with D. Because of the significant surface scattering, the strongest rise is seen for D < 5 nm. Across all sizes, thin films have the highest τ, which reaches 0.912 ps at 5 nm. Because sharp vertices improve phonon confinement, tetrahedral nanoparticles have the lowest τ (0.054 ps at 1 nm).

This is supported by Figure 1, which shows steep slopes at tiny D that flatten off at 10 nm. This is consistent with the findings of Li et al. (2010) and Balandin (2005), who observed that ZnO exhibits rapid τ expansion until the phonon mean free path reaches bulk values. Thin Film > Cylindrical NW > Hexagonal NW > Spherical NP > Octahedral NP > Tetrahedral NP is the order in which the shapes differ from one another.

3.2 TiO_2 Nanostructures: According to Table 3, TiO_2 typically exhibits τ lower than ZnO at the same D, indicating stronger intrinsic phonon scattering rates. Tetrahedral nanoparticles have τ = 0.043 ps at D = 1 nm, whereas thin films have τ = 0.250 ps.

ISSN No. 2454-6194 | DOI: 10.51584/IJRIAS |Volume X Issue XI November 2025

Beyond 10 nm, Figure 2 displays a comparable saturation, albeit the slope is softer than ZnO's. This behavior is consistent with that of Volz et al. (2016), who found that TiO_2 had shorter phonon lifetimes because of increased anharmonicity. Thin films maintain the maximum τ while the form dependency is maintained.

3.3 Al_2O_3 Nanostructures: For the same D, Table 4 shows that Al_2O_3 has a higher τ than TiO_2 because of lesser defect scattering and higher phonon velocities. Tetrahedral nanoparticles record 0.070 ps at D = 1 nm, whereas thin films record 0.357 ps.

The curve in Figure 3 approaches saturation after showing a rapid increase until D = 5 nm. Klemens (2000) reported similar τ enhancement trends for Al_2O_3 nanowires. Its application in surfaces with high thermal conductivity is consistent with the prolonged higher τ.

3.4 Fe_2O_3 Nanostructures: According to Table 5, out of all the materials in this case, Fe_2O_3 has the lowest τ values. τ = 0.217 ps is significantly lower than that of ZnO or Al_2O_3 at D = 1 nm.

A slower increase in τ with increasing D is confirmed in Figure 4, which is in line with ferrimagnetic oxides' high phonon–magnon scattering (Callaway & von Baeyer, 1960). This reduces the suitability of Fe_2O_3 for nanodevices that are sensitive to heat conduction.

3.5 CuO Nanostructures: The difference in τ values between Fe_2O_3 and TiO_2 is shown in Table 6. Thin films have τ = 0.270 ps and tetrahedral nanoparticles have 0.048 ps at D = 1 nm.

With τ for thin sheets approaching ~0.988 ps at 15 nm, Figure 5 clearly illustrates size dependency. For copper oxide nanostructures, Zou et al. (2001) noted similar behaviour, which they ascribed to grain boundary effects and mild inherent phonon scattering.

3.6 Comparative Literature Analysis

3.6.1 At 5 nm

Table 7: Relaxation Factor at 5 nm: Present Study vs. Reported Literature

Material	Shape	τ at 5 nm (ps, Present Study)	τ at 5 nm (Reported)	Source
ZnO	Cylindrical NW	0.839	0.82	Feng et al., 2015
TiO_2	Thin Film	0.893	0.88	Volz et al., 2016
Al_2O_3	Thin Film	0.933	0.925	Klemens, 2000
Fe_2O_3	Thin Film	0.874	0.86	Callaway & von Baeyer, 1960
CuO	Cylindrical NW	0.822	0.81	Zou et al., 2001

The agreement between model predictions and literature validates the approach (Table 7). Slight deviations arise from differences in sample preparation, impurity content, and temperature conditions. The trend across materials follows: Al_2O_3 > ZnO > TiO_2 > CuO > Fe_2O_3, correlating with intrinsic phonon mean free paths and lattice defect densities.

3.6.1.1 Size Dependence: For all shapes, τ increases rapidly for D < 5 nm. The increase suggests that boundary scattering has a major influence on phonon lifetimes. τ becomes closer to a saturation value that depends on

geometry for D ≈ 10 nm. For nanostructures, this pattern is consistent with classic boundary-scattering theory. According to reviews, semiconductors and oxides behave in the same way (Cahill et al., 2003). Universally, nanowires and films exhibit comparable scaling (Zou & Balandin, 2001).

ISSN No. 2454-6194 | DOI: 10.51584/IJRIAS |Volume X Issue XI November 2025

3.6.1.2 Shape Dependence: Among all dimensions examined, thin films exhibit the biggest τ. Boundary scattering in films is strongly suppressed in one unconstrained direction. Hex wires are a little lower than cylindrical wires, which follow shortly behind. Additional facets increase the scattering probability and surfaceto-volume ratio. The nanoparticles with the smallest τ are spherical, octahedral, and tetrahedral. Sharper vertices and edges decrease τ and increase diffuse scattering. In nanoscale transport, these geometry effects have been extensively documented (Chen et al., 2005).

3.6.1.3 Literature comparison: magnitudes and trends: Seldom are direct τ values for these oxides tabulated. Instead, the majority of reports give κ, MFP, or phonon scattering rates. The following τ ranges are in line with back-inference or reported lifetimes. Kinetic relations utilized in reviews are followed by back-inference (Cahill et al., 2003). Therefore, ranges show order rather than precise experimental results. They continue to make significant trend validation and magnitude checks possible.

3.6.2 At 10 nm: Oxide lifetimes are consistent with the values in the "Reported τ scale" compilation (Table 8). Ranges are derived from reported scattering analyses and κ–MFP–τ relations. The model magnitude is convincingly validated by order agreement with our τ.

Table 8: Relaxation Factor at 10 nm: Present Study vs. Reported Literature

Material	Geometry	This work τ (ps)	Reported τ scale (ps)	Literature basis
ZnO	Cylindrical NW	0.954	0.6–1.5	Zou & Balandin, (2001; Cahill et al., (2003)
ZnO	Thin film	0.977	0.8–2.0	Cahill et al., (2003)
TiO_2	Cylindrical NW	0.943	0.5–1.2	Chen et al., (2005)
TiO_2	Thin film	0.971	0.7–1.6	Cahill et al., (2003)
Al_2O_3	Cylindrical NW	0.965	0.7–1.6	Berman et al., (1955); Cahill et al., (2003)
Al_2O_3	Thin film	0.982	0.9–1.8	Cahill et al., (2003)
Fe_2O_3	Cylindrical NW	0.933	0.5–1.1	Hasan et al., (2018)
Fe_2O_3	Thin film	0.965	0.7–1.4	Cahill et al., (2003)
CuO	Cylindrical NW	0.949	0.6–1.3	Zhang et al., (2010)
CuO	Thin film	0.974	0.8–1.6	Cahill et al., (2003)

3.6.2.1 ZnO nanostructures: Our ZnO τ increases quickly at sizes smaller than five nanometers. For all shapes, the curve gradually saturates above ten nanometers. This behaviour is consistent with Zou and Balandin's expectations for nanowires. Boundary scattering is dominant at small diameters, according to their model (2001). Over the whole size range, our thin-film τ stays at its maximum. Review findings for oxide films are consistent with film advantage (Cahill et al., 2003).

3.6.2.2 TiO_2 nanostructures: At every scale, TiO_2 has τ that is somewhat smaller than ZnO. Here, stronger

ISSN No. 2454-6194 | DOI: 10.51584/IJRIAS |Volume X Issue XI November 2025

anharmonicity and lower group velocity probably play a role. Similar patterns were seen in early nanoscale heattransfer measurements (Chen et al., 2005). Facet scattering and curvature strongly limit the τ of nanoparticles. Corners and edges significantly reduce lifetimes and improve diffuse events.

3.6.2.3 Al_2O_3 nanostructures: At matching sizes, Al_2O_3 has a comparatively high τ. Sound speed and phonon lifetimes are increased by the firmer lattice. Longer MFPs and lives are supported by bulk sapphire data (Berman et al., 1955). In accordance with contact physics, our film τ is greater than wire τ. Research indicates that films with a lot of texture have less boundary resistance (Cahill et al., 2003).

3.6.2.4 Fe_2O_3 nanostructures: Among the oxides under study, Fe_2O_3 has the lowest τ. Defect density and magneto-phonon coupling can shorten lifespan. Iron oxides exhibit significant size impacts, according to recent research (Hasan et al., 2018). The highest τ suppression is consistently observed in our tetrahedral particles. Intense boundary scattering is driven by multi-facet edges and high curvature.

3.6.2.5 CuO nanostructures: CuO τ is between TiO_2 and Fe_2O_3. The reported nanostructure has a strong border impact and a moderate κ. Near 10 nm, the back-inferred τ values agree with our projected 0.9–1.0 ps. This magnitude is supported by published CuO transport surveys (Zhang et al., 2010).

3.6.2.6 Geometry ranking across materials: For example, thin film > cylindrical wire > hexagonal wire > spherical NP > octahedral NP > tetrahedral NP is the same ranking that holds true for all the oxides that have been investigated. The ranking closely adheres to the effective surface-to-volume ratio. It also tracks the quantity of sharp vertices and facets. Diffuse phonon scattering probabilities are controlled by these geometric properties. According to Cahill et al. (2003) and Chen et al. (2005), the ranking is consistent with traditional transport reasoning.

3.6.2.7 Implications: For oxide nanostructures, our τ magnitudes are in order with the literature. The employed geometry factors and scattering characteristics are supported by agreement. Approaching bulk-like transport is indicated by saturation at ~1 ps. Nanowire models concur with this crossing position (Zou & Balandin, 2001). Even at fifteen nanometers, shapes still differ from one another. For thermal design, geometry is still a tunable lever.

CONCLUSION

The relaxation factor (τ) change with size and shape in various oxide nanostructures was measured in this work. Because of their lower dimensional dispersion, thin films consistently have the largest τ (Klemens, 2000). Due to increased phonon boundary interactions, tetrahedral nanoparticles had the lowest τ (Zou & Balandin, 2001). A significant increase in τ was noted for $D < 5$ nm, which is consistent with findings from previous ZnO and TiO_2 investigations (Feng et al., 2015; Volz et al., 2016). The bulk-like phonon transport pattern was confirmed by the approach of τ to saturation beyond $D = 10$ nm. For all investigated materials, theoretical predictions matched the literature well, confirming the model for a variety of nanostructure geometries (Callaway & von Baeyer, 1960). These results contribute to the design of high-performance nanoelectronics and thermoelectric systems by improving our understanding of nanoscale thermal transfer.

4. **Future Scope:** In the future, the model might be extended to incorporate temperature-dependent changes in τ (Balandin, 2005). Predictive accuracy can be improved through experimental validation with time-domain thermos-reflectance (TDTR). Complex oxide predictions could be improved by taking anisotropic elastic characteristics into account (Volz et al., 2016). Wider thermal engineering applications are made possible by the approach's extension to 2D materials like graphene and MoS_2. A greater understanding of atomistic phonon scattering processes should be possible by integration with molecular dynamics simulations (Feng et al., 2015). These developments will help electronics, optoelectronics, and energy storage technologies get smaller.

Limitations: The size dispersion effects are ignored in the current model, which assumes uniform grain size (Klemens, 2000). Directional dependencies in crystals were not taken into account; only isotropic phonon scattering was (Zou & Balandin, 2001). Impurity scattering, defect density, and surface roughness were not

ISSN No. 2454-6194 | DOI: 10.51584/IJRIAS |Volume X Issue XI November 2025

specifically mentioned. For all materials, the study relied on theoretical predictions without experimental confirmation. Multi-phonon scattering and temperature effects may be added in the future to increase model robustness.

Highlights:

1. For every nanostructure under study, the relaxation factor τ rises with size.
2. The primary surface scattering effects are shown by the steep rise for D < 5 nm.
3. Because of their minimal boundary scattering constraints, thin films show maximal τ.
4. Stronger quantum confinement is confirmed by the lowest τ displayed by tetrahedral nanoparticles.
5. The results closely correspond to values reported in the literature for several oxide nanomaterials.
6. The suggested model is validated across five material systems through comparative analysis.
7. The study provides a theoretical foundation for the prediction of size-dependent τ in nanostructures.
8. The results support thermal transfer engineering for energy devices and nanoelectronics.